

Effect of large magnetocrystalline anisotropy on the spin wave linewidth in Zn–Y hexagonal ferrite

Alexey V. Nazarov^{a)} and Carl E. Patton

Department of Physics, Colorado State University, Fort Collins, Colorado 80523

(Received 5 December 2002; accepted 15 March 2003)

The oblique pumping spin wave instability threshold microwave field amplitude h_{crit} was measured as a function of the static field for both in-plane and out-of-plane static fields for a thin disk of Mn substituted Zn–Y ($\text{Ba}_2\text{Zn}_2\text{Fe}_{12}\text{O}_{22}$) easy plane hexagonal ferrite at 16.7 GHz. Theoretical fits to the in-plane static field data gave a single value of 12.8 Oe for the spin wave linewidth ΔH_k . The best overall fits were for a critical spin wave mode wave number k close to zero and there was no correlation with the critical mode propagation directions. The fitted ΔH_k for the out-of-plane static field geometry was found to increase with the out-of-plane magnetization angle, but showed no correlation with the critical mode propagation directions. These critical modes had $k \approx 0$ as well. The fitted ΔH_k increased from the in-plane field value of 12.8 Oe to a value of 21 Oe at the maximum accessible magnetization angle of 70° relative to the disk plane. This increase in spin wave damping with the out-of-plane angle is attributed to spin orbit coupling. © 2003 American Institute of Physics. [DOI: 10.1063/1.1572971]

I. INTRODUCTION

Hexagonal ferrite materials offer advantages for millimeter wave applications because of the large anisotropy.¹ High power microwave applications require an understanding of the spin wave instability threshold power levels and the corresponding spin wave linewidth ΔH_k which is a measure of the spin wave damping. Up to now, high power analyses for Zn–Y materials have generally taken ΔH_k to be isotropic.^{2–5}

Recent high power Zn–Y measurements for static fields out of the easy plane indicated an increase in the spin wave linewidth relative to the in-plane field case. The objective of this work was to perform a series of first order spin wave instability threshold field h_{crit} measurements for oblique pumping with both in-plane and out-of-plane static fields, and determine the spin wave linewidth for all of these configurations. Oblique pumping corresponds to field geometry for which the linearly polarized microwave field and the static magnetization have a relative angle between zero and 90° .⁶ In these experiments, the pumping angle causes large changes in the half frequency critical modes responsible for the instability. The results indicate that while ΔH_k is relatively insensitive to the particular critical mode for the instability, it is very sensitive to movements of the static magnetization from in plane to out of plane.

II. EXPERIMENT

The samples for the measurements consisted of thin disks fabricated from bulk single crystal platelets of Zn–Y hexagonal ferrite with Mn substitutions. The specific composition was $\text{Ba}_2\text{Zn}_{1.82}\text{Fe}_{11.83}\text{Mn}_{0.68}\text{O}_{21.2}$. The saturation induc-

tion $4\pi M_s$ was 2.33 kG and the effective anisotropy field H_A was -9.4 kOe.⁵ The data in this article are presented for a representative easy c -plane disk sample with a diameter of 2.32 mm and a thickness of 0.19 mm. The disk had a ferromagnetic resonance (FMR) linewidth of 13 Oe at 9.5 GHz, as measured for an in-plane static field. This value is reasonably small for this material.^{4,7}

The high power measurements were made with a pulsed reflection cavity spectrometer at a nominal frequency of 16.7 GHz. The high power thresholds were obtained from the power at which the reflected pulses showed a discernable nonlinear response. The measurements were made with the sample in the center of the standard TE_{102} rectangular cavity. The power thresholds were converted to threshold microwave field amplitudes under the assumption of an unperturbed cavity mode applicable to small samples. Details of the method are given in Refs. 5 and 8.

The spin wave instability threshold fields were measured versus static field for two different oblique pumping arrangements with the static field in plane and out of plane, respectively. Plots of h_{crit} vs H are typically called “butterfly curves.” The microwave magnetic field \mathbf{h} was kept in plane for both cases. Figures 1 and 2 show the field arrangements. For the in-plane field oblique pumping (IPFOP) geometry of Fig. 1, the static field \mathbf{H} is in plane at an angle ϕ_h relative to the in-plane \mathbf{h} . In this case, the static magnetization \mathbf{M} is parallel to \mathbf{H} . For the out-of-plane field oblique pumping (OPFOP) geometry of Fig. 2, \mathbf{H} is rotated out of the disk plane but maintained in the plane defined by the disk normal and the microwave field \mathbf{h} , the x - z plane in the figure. In this case, the field \mathbf{H} is set at some out-of-plane angle, taken as θ_H , relative to the disk normal. The magnetization vector \mathbf{M} is pulled out of the disk plane. For purposes of this analysis, \mathbf{M} is taken to be in the x - z plane in Fig. 2 and at an angle θ_M relative to the disk normal. At static equilibrium, θ_M may be obtained from the static equilibrium condition

^{a)}Author to whom correspondence should be addressed. Present address: National Institute of Standards and Technology, Boulder, CO 80303; electronic mail: nazarov@boulder.nist.gov

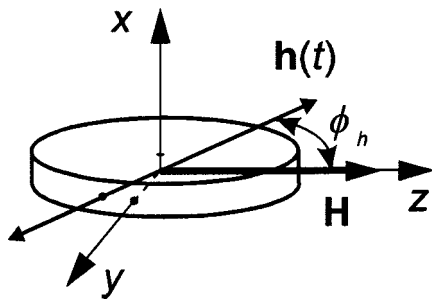


FIG. 1. Geometry for the in-plane field oblique pumping (IPFOP) case. The disk is in the y - z plane of the (x, y, z) coordinate frame. The external static field \mathbf{H} is along z . The linearly polarized microwave field $\mathbf{h}(t)$ is in the y - z plane at an angle ϕ_h relative to \mathbf{H} .

$$2H \sin(\theta_H - \theta_M) = [4\pi M_s(3N_{ip} - 1) + H_A] \sin(2\theta_M), \tag{1}$$

where N_{ip} is the in-plane demagnetizing factor for the disk. The two oblique pumping geometries described above allow one to access different instability processes. In the IPFOP case, the oblique pumping angle ϕ_h is a direct control parameter in the experiment. The critical mode polar and azimuthal spin wave propagation angles both change with ϕ_h . In the OPFOP case, the situation is more complicated. When θ_H is nonzero, \mathbf{H} , \mathbf{h} , and \mathbf{M} are in the x - z plane and the pumping geometry is well defined. However, at $\theta_H = 0$ for any applied field below $|H_A| + 4\pi M_s$, any small misalignment will affect the actual pumping angle between \mathbf{h} and \mathbf{M} . Since such small misalignments cannot be controlled, any theoretical fits must take this variability in the pumping angle into consideration. These considerations will be used below for the data analysis in the OPFOP case.

III. RESULTS AND DISCUSSION

A. Butterfly curves for an in-plane static field

Figure 3 shows the in-plane field oblique pumping results for h_{crit} as a function of the external static field H . Data and theoretical fits are shown for three ϕ_h values, zero, 45° , and 90° , as indicated. The symbols show the data. The solid lines show curves obtained from the theory of Ref. 9 for a

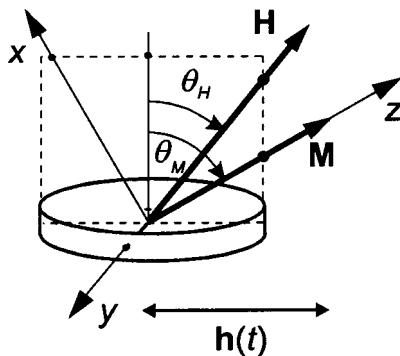


FIG. 2. Geometry for the out-of-plane field oblique pumping (OPFOP) case. The external static field \mathbf{H} is in the x - z plane at an angle θ_H relative to the disk normal. The static magnetization \mathbf{M} is in the x - z plane at an angle θ_M relative to the disk normal. The linearly polarized microwave field $\mathbf{h}(t)$ is in the x - z plane and in the disk plane.

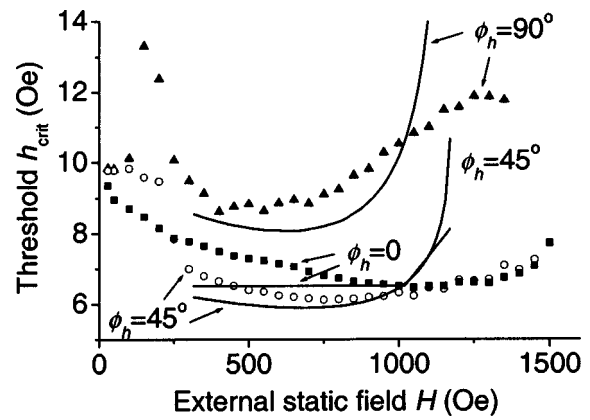


FIG. 3. In-plane field oblique pumping (IPFOP) threshold h_{crit} as a function of the external static field H for the Zn–Y disk with microwave excitation at 16.7 GHz. The graphs show results for values of the in-plane oblique pumping angle ϕ_h , as indicated. The symbols show the data. The solid lines show computed results for a constant spin wave linewidth of 12.8 Oe.

constant spin wave linewidth ΔH_k value of 12.8 Oe. The lower limit fields for the calculated butterfly curves were determined from the onset of demagnetizing effects apparent from the data at $H = H_d \sim 300$ Oe for all three sets of data. This H_d value indicates an N_{ip} demagnetizing factor of about 0.13. This empirical N_{ip} value is about a factor of 2 larger than estimates based on the Osborn formulas for ellipsoids. The model calculations for the data analysis discussed below use this empirical value.

The important results in Fig. 3 concern the mid-range of static fields between about 300 and 1000 Oe. One can see that for this middle range of fields, the average threshold values from the measurements and the computed curves follow the same trend. The thresholds at $\phi_h = 0$ and $\phi_h = 90^\circ$ are both larger than the thresholds for $\phi_h = 45^\circ$. The qualitative tracking between the data and the theory for a single value of the spin wave linewidth is significant. This tracking and the critical modes implicit in the computed curves in Fig. 3 will be discussed in more detail shortly.

It is worth noting that the h_{crit} data in Fig. 3 extend to somewhat higher fields than indicated by the calculated curves. This is an effect of nonuniform demagnetizing fields. The theoretical curves diverge or truncate at the high field limit for which there are no available spin waves at one-half the pumping frequency. As noted above, the computed curves were obtained under the assumption of a uniform demagnetizing field of about 300 Oe. However, the sample had an aspect ratio of nearly 10:1 and a corresponding inhomogeneous internal field, especially at the edges. If one assumes that this inhomogeneity is on the order of the demagnetizing field itself, one can qualitatively explain the extension of the threshold data to the fields indicated. This field extension is about 300 Oe. These estimates are in a good agreement with the data on thin plate samples with different dimensions.⁸

The effect of the demagnetizing fields in Zn–Y materials or other easy plane hexagonal ferrites has not been treated theoretically. The spin wave instability theory implies a uniformly magnetized sample which is valid for ellipsoidal shapes only. The spin wave instability processes occur in the local regions of the sample and the regions with the inhomogeneous

geneous fields may have lower threshold. In these regions, \mathbf{M} is declined from the in-plane direction. It will be shown later in Sec. III B that when \mathbf{M} deviates from the in-plane direction and θ_M decreases the h_{crit} data extend to higher fields. The actual measured extension depends on the sensitivity of the measurement system because the regions with the inhomogeneous fields are quite small compared to the sample volume. Therefore, one can only estimate the effect of the nonuniform demagnetizing fields in a disk sample. This is a technological difference between a model and a real sample. Note that nonuniform demagnetizing fields do not affect the FMR linewidth significantly because the total volume with the inhomogeneous fields is much smaller than the rest of the sample.^{5,10}

Further comments are needed at this point on the critical modes associated with the theoretical curves in Fig. 3. As noted above, all of the theoretical curves were obtained through the usual minimization procedure described in Ref. 9 to obtain the lowest threshold at a given static field. The $\phi_h=0$ case corresponds to parallel pumping. Here, the computed curve is flat below $H=1000$ Oe and there is a small truncated linear segment for $1000 \text{ Oe} < H < 1200$ Oe. The critical mode k values range from zero at $H=1000$ Oe to about 3.5×10^5 rad/cm at $H=300$ Oe. Over this full range, critical mode polar and azimuthal propagation angles, taken as θ_k and ϕ_k , remain constant at 90° and zero, respectively. Note that these angles are measured relative to the (x, y, z) coordinate system in Fig. 1. Critical modes at $\theta_k=90^\circ$ and $\phi_k=0$ correspond to a wave vector \mathbf{k} which is normal to the disk plane.

The situation for $\phi_h=45^\circ$ and $\phi_h=90^\circ$ is quite different. Here, both computed curves are concave upward over the entire range of fields for the evaluations. Furthermore, the minimum threshold critical modes have $k=0$ over the 300–1000 Oe field range of interest, but the critical mode polar propagation angle θ_k changes with field. For the $\phi_h=90^\circ$ case, θ_k decreases from 15° to 40° as H decreases from 1000 to 300 Oe. The azimuthal propagation angle ϕ_k remains constant, but is now at 90° . The propagation directions for these low k modes are in the plane of the disk sample. The critical mode response for $\phi_h=45^\circ$ is similar. Note that zero k in the context of Ref. 9 really means that the critical mode wave number is in the range of 10^4 rad/cm. These low k modes are available in the entire field range because the separation between top and bottom spin wave dispersion branches in Zn–Y is much larger than in isotropic ferrites.⁵

There are two crucial points from the above critical mode results. First, in-plane oblique pumping produces a wide range of critical mode wave numbers and propagation angles. Second, one can use the theory with these different critical mode properties taken into account and obtain a reasonable match to the data for *one and the same* ΔH_k value of 12.8 Oe.

Further comments and analyses are in order for the $\phi_h=0$ results in Fig. 3. It is worth noting that for this case only, the computed butterfly curve for the $300 \text{ Oe} < H < 1000$ Oe field range shows a completely flat response. At the same time, the data show an h_{crit} which increases with decreasing

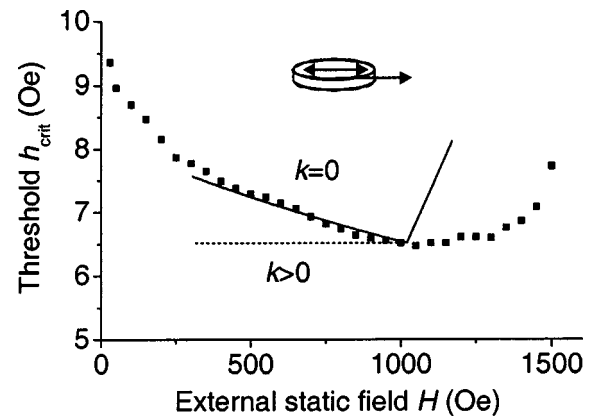


FIG. 4. Parallel pumping threshold h_{crit} as a function of the external static field H for the Zn–Y disk with microwave excitation at 16.7 GHz. The solid squares show the same $\phi_h=0$ data as in Fig. 3. The solid line shows the results of the numerical calculations with the critical mode wave number k constrained to zero. The dotted line shows the corresponding computed curve from Fig. 3.

field over this field range. This same result was presented in Fig. 2 of Ref. 5, and it was suggested that a k -dependent ΔH_k was responsible for the discrepancy between the data and the theory.¹¹ However, the new data for $\phi_h=45^\circ$ and $\phi_h=90^\circ$ suggest an alternative explanation. Recall that the minimum threshold critical modes for these two cases had $k=0$ and the trend of the calculated curves match the data, more or less. Based on these results, additional computations were done for the $\phi_h=0$ parallel pumping case, but with the wave number constrained to $k=0$. It was found that this constraint actually yielded a better fit to the data, even with the same $\Delta H_k=12.8$ Oe used for the curves in Fig. 3.

Figure 4 shows the data from Fig. 3 for $\phi_h=0$ only and a new computed curve subject to the $k=0$ constraint. The format is the same as for Fig. 3. The solid squares show the same data as in Fig. 3. The solid curve shows the calculated butterfly curve with the $k=0$ constraint for the minimum threshold critical mode. The dashed curve shows the previous calculated curve without this constraint and as discussed above. As before, the computed curves were obtained for a k -independent ΔH_k value of 12.8 Oe.

Figure 4 clearly shows that the $k=0$ constraint gives a nearly perfect fit to the data over the central field interval from 300 to 1000 Oe. As discussed above, demagnetizing effects become important for fields below and above these limits. This fit has several ramifications. First, the good fit for $k=0$ modes compared to the poor fit for an unconstrained k , suggests that the usual explanation for the increase in h_{crit} with decreasing field in terms of a k -dependent ΔH_k is not correct in the current situation. Second, the critical mode fits, even with k constrained to be zero, still yield a variation in direction of the vector \mathbf{k} .

Keep in mind that, as noted above, the $k=0$ constraint only means that the magnitude of k is in the range of 10^4 rad/cm. The solid line in Fig. 4 corresponds to a critical mode polar angle θ_k of 90° and an azimuthal angle ϕ_k which increases from 0 to 40° as H decreases from 1000 to 300 Oe. The corresponding propagation directions are out of plane. Considered as a whole, the fits to the $\phi_h=0$ data in Fig. 4

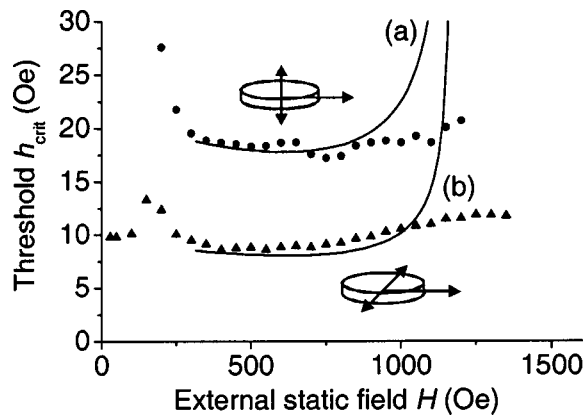


FIG. 5. Perpendicular pumping threshold h_{crit} as a function of the in-plane external static field H for the Zn-Y disk with microwave excitation at 16.7 GHz. The graphs show results (a) for out-of-plane and (b) for in-plane perpendicular pumping, as indicated by the diagrams. The symbols show the data. The solid lines show computed results for a constant spin wave linewidth of 12.8 Oe.

and the results in Fig. 3 for $\phi_h = 45^\circ$ and $\phi_h = 90^\circ$ show that one value of ΔH_k gives a reasonable butterfly curve match between theory and experiment for a wide range of critical mode propagation directions.

There is one further implication of the results in Fig. 4. The fact that one obtains a good fit to the data for $\phi_h = 0$ with k constrained to zero suggests that there must be a strong k dependence for ΔH_k . Keep in mind that the minimum threshold critical modes for a k -independent spin wave linewidth have a nonzero k . Why would the system “prefer” to have $k=0$ critical modes for the $\phi_h = 0$ parallel pumping case? A strongly k -dependent ΔH_k provides a plausible answer to this question. This effect is not accessible for the $\phi_h = 45^\circ$ or $\phi_h = 90^\circ$ configurations because the critical modes are at $k=0$ in the first place.

Figure 5 shows additional results for the perpendicular pumping case with the microwave field perpendicular to the slab plane. The format is the same as for Figs. 3 and 4. The upper data set and theoretical curve, labeled as (a), show the results for a microwave field direction which is perpendicular to the slab plane, as indicated. The lower data set and theoretical curve, labeled (b), show the result from Fig. 3 for $\phi_h = 90^\circ$ and in-plane perpendicular pumping. As before, the theoretical curve in (a) was obtained for $\Delta H_k = 12.8$ Oe. The minimum threshold critical modes were identical with those obtained with the $\phi_h = 90^\circ$ in-plane pump. These results show that the same kind of match-up shown in Figs. 3 and 4 can be obtained for out-of-plane perpendicular pumping as well, and *all for the same value of the spin wave linewidth* as used before.

B. Butterfly curves for an out-of-plane static field

Turn now to the OPFOP results. As noted above, this pumping configuration with the static field out of plane is much more complicated than in the IPFOP case. In reference to the OPFOP configuration in Fig. 2, consider the effect of the field \mathbf{H} on the orientation of the vector magnetization \mathbf{M} . The figure shows the ideal situation for which \mathbf{H} , \mathbf{M} , and the

in-plane microwave field \mathbf{h} are all in the x - z plane. When H is small and θ_H is larger than about 10° , the vector \mathbf{M} will be nearly in plane and the pumping configuration will be essentially the same as in the IPFOP case with parallel pumping at $\phi_h = 0$. If H is then increased, \mathbf{M} will gradually be pulled out of the film plane and the pumping configuration will change from pure parallel pumping to oblique pumping. This evolution in the pumping configuration results in significant changes in the critical modes and the shape of the butterfly curve, especially at high field.⁹

For small θ_H , however, the change in the pumping configuration with a change in H is more involved. In order to show the problem, consider the limit of a small H at $\theta_H = 0$. For a small H , \mathbf{M} will be in plane. However, the actual in-plane direction for \mathbf{M} will be controlled by whatever small deviation of the actual field direction from the disk normal. In reference to Fig. 2, this \mathbf{H} will be along the indicated vertical reference line at $\theta_H = 0$. If the film happens to be tilted by some small angle so that the film normal points out of the page by some small angle, for example, then the in-plane \mathbf{M} will be perpendicular to the in-plane \mathbf{h} . Since any such small misorientation of the film cannot be known, the actual pumping configuration in the low field limit could range from parallel to perpendicular, or any angle in between. One may define a misorientation angle ϕ_H as the angle between the projection of \mathbf{H} onto the film plane and the in-plane microwave field \mathbf{h} . In the low field limit with \mathbf{M} in plane, this angle will also correspond to the angle between \mathbf{M} and \mathbf{h} . As H is increased and \mathbf{M} is pulled out of the disk plane, the angle between \mathbf{M} and \mathbf{h} and the corresponding pumping configuration will move uniformly from ϕ_H to an angle close to $90^\circ - \theta_H$.

The practical implications of the above misorientation effect for fits to experiment in the OPFOP case are clear. One cannot assume a particular orientation between the in-plane \mathbf{M} and the in-plane \mathbf{h} in the limit of low fields when \mathbf{H} is close to $\theta_H = 0$. In order to compare theoretical butterfly curves with data, it will be necessary to examine the responses for a range of ϕ_H values. The effect of ϕ_H on the theoretical curves and the correlation with the data will be clear from the results below.

Figure 6 shows representative OPFOP butterfly curve data along with three computed curves. These particular results are for a static field direction close to the perpendicular orientation at an experimental θ_H setting of 5° . The solid circles show the data. The dashed and solid lines show the computed results. The upper limit of the data at about $H = 10.3$ kOe corresponds to a truncation point. At higher fields, there are no available half frequency spin waves and there is no first order h_{crit} threshold. The abrupt jump in h_{crit} for $H < 2$ kOe and low field peak at $H \approx 1$ kOe are due to demagnetizing effects. The h_{crit} value of 10 Oe at $H = 0$ matches the IPFOP thresholds at zero field for all three data sets in Fig. 3.

As in Sec. III A, the computed curves in Fig. 6 were obtained from the formalism of Ref. 9 for a constant spin wave linewidth ΔH_k value of 12.8 Oe. The solid curve was obtained in two steps. First, the angle θ_H was treated as an adjustable parameter and used to force the computed h_{crit}

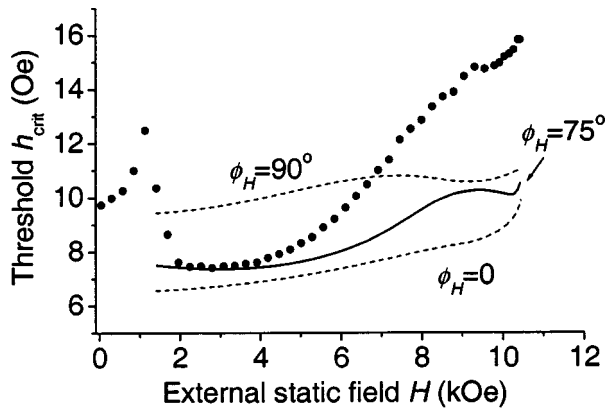


FIG. 6. Out-of-plane field oblique pumping (OPFOP) threshold h_{crit} as a function of the external static field H for the Zn-Y disk with in-plane microwave excitation at 16.7 GHz. The solid circles show the data for a field angle $\theta_H=5^\circ$ relative to the disk normal. The solid and dashed lines show computed results for a constant spin wave linewidth of 12.8 Oe, an adjusted θ_H value of 6.7° , and in-plane misorientation angle ϕ_H values, as indicated.

curve to truncate at the same high field H value as the data. This fitted θ_{H-Fit} value was 6.7° . Second, the misorientation angle ϕ_H defined above was adjusted to force the low field h_{crit} values to match the data. This fitted ϕ_H value was 75° . Figure 6 also shows two dashed curves. These curves were computed for ϕ_H values of zero and 90° in order to bracket the full range of possible misorientation angles as discussed above.

The data and the calculated curves in Fig. 6 indicate a very different result for the OPFOP geometry than for the IPFOP case. First of all, one can see that as the field goes above about 7 kOe, the measured thresholds rise above the highest computed curve for $\Delta H_k=12.8$ Oe. At the same time, one can see that the solid line computed curve for $\phi_H=75^\circ$ is matched nicely to the low field data below about 4 kOe, where \mathbf{M} is essentially in plane. Note also that the fitted θ_{H-Fit} value of 6.7° allows the computed truncation points at $H=10.4$ kOe to fall right at data truncation field limits. These consistent fits indicate that the model is essentially correct. One is left, therefore, with a problem of how to explain the clear and rapid increase in h_{crit} when the out-of-plane field H increases and \mathbf{M} moves out of plane as well.

One obvious strategy to resolve this problem would be to consider a wave vector or critical mode dependence for ΔH_k . One can check this approach empirically by considering data similar to those shown in Fig. 6, but for a range of experimental θ_H values. For each set of data, one can use the increase in the measured h_{crit} above the computed curve for $\Delta H_k=12.8$ Oe to estimate the needed increase in the spin wave linewidth as H is increased and \mathbf{M} is pulled out of plane. One can then look for correlations between these changes and the changes in the critical mode wave vector parameters k , θ_k , and ϕ_k .

This analysis was done for three experimental θ_H values, zero, 5° , and 10° . The 5° data were the same as discussed above. The two-step fit procedure to determine the actual θ_H and ϕ_H values for comparison with theory was the same as given above. It was found that the ΔH_k vs H response was essentially the same for all of the data. At the same time,

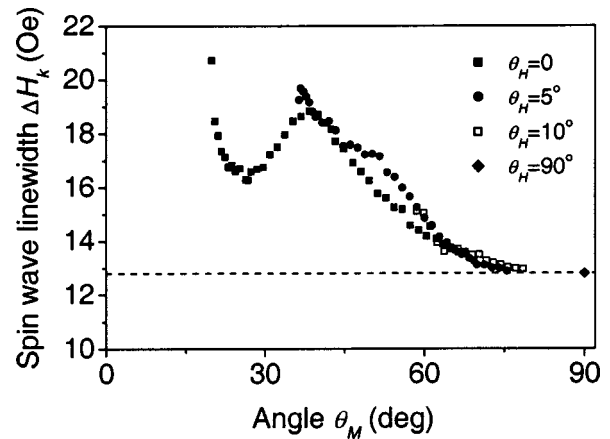


FIG. 7. Spin wave linewidth ΔH_k vs the static magnetization equilibrium angle θ_M for the Zn-Y disk at 8.35 GHz. The symbols show ΔH_k values extracted from the h_{crit} data for experimental θ_H values, as indicated. The horizontal dashed reference line corresponds to a constant ΔH_k at 12.8 Oe.

however, the critical mode response was quite different for the three θ_H values examined. The fitted ϕ_H values were all nonzero. The critical mode k values were all zero, as in the IPFOP case. However, the calculated critical mode angles θ_k and ϕ_k varied significantly with θ_H and with field. These results appear to exclude a \mathbf{k} -dependent ΔH_k as the origin of the h_{crit} response shown in Fig. 6. This conclusion is also consistent with the IPFOP results of the previous section.

It is important to keep in mind that the $k=0$ critical mode condition makes it impossible to draw any conclusions about the actual k dependence of ΔH_k . Recall that the IPFOP $\phi_H=0$ results suggested a strong k -dependent spin wave linewidth. But these are the only data which allow for any such suggestion.

However, the fact that the ΔH_k vs H response from all of the h_{crit} data for all three θ_H values falls on a common curve does provide a clue to explain the problematic h_{crit} increase as \mathbf{M} is pulled out of plane. The important physical parameter here is, in fact, the magnetization angle θ_M and not the external field. The common ΔH_k vs H response converts to a common ΔH_k vs θ_M response. It is this response which provides an indication of the new physical results for the OPFOP case. A ΔH_k vs θ_M display was obtained from the ΔH_k fit data discussed above and θ_M was calculated from the static equilibrium condition of Eq. (1) for the applicable θ_{H-Fit} values. These θ_M values were verified from vibrating sample magnetometer measurements of the vector magnetic moment for the given Zn-Y disk.

The full ΔH_k vs θ_M results are shown in Fig. 7. The solid squares, solid circles, and open squares show the results for the three experimental θ_H values of zero, 5° , and 10° , as indicated. The single solid diamond point at $\theta_M=90^\circ$ corresponds to the parallel pumping result at $H=1$ kOe, taken from Fig. 4. The horizontal dashed line for $\Delta H_k=12.8$ Oe is included to show a point of reference for the constant spin wave linewidth from the IPFOP analysis.

One can see from Fig. 7 that the spin wave linewidth increases significantly as the magnetization \mathbf{M} is pulled out of the easy plane. For θ_M values above 70° or so, ΔH_k is at

its minimum value which has been matched to the IPFOP value of 12.8 Oe according to the fitting procedure discussed above. As θ_M falls below 70° , ΔH_k is seen to increase. The spin wave linewidth then shows a broad peak at $\theta_M \sim 40^\circ$ and a maximum ΔH_k of about 19 Oe. As θ_M is further reduced, this peak is followed by a local minimum at $\theta_M \sim 25^\circ$ with $\Delta H_k \sim 16.5$ Oe. For $\theta_M < 20^\circ$, ΔH_k increases rapidly. The smallest out-of-plane magnetization angle accessible in the experiments was at $\theta_M \sim 20^\circ$. At this point, the fitted ΔH_k value was about 21 Oe. It is important to note that the full response evident in Fig. 7 is derived from the data for $\theta_H = 0$ only. The accessible θ_M values from the $\theta_H = 5^\circ$ and $\theta_H = 10^\circ$ data show only the increase as \mathbf{M} is initially pulled out of plane. These data are too limited to show the full profile.

While initially unexpected, the fact that the spin wave linewidth changes as the magnetization vector is pulled out of plane is not surprising. The relaxation processes which give rise to ΔH_k in the first place derive from fundamental magnon–magnon and magnon–phonon interactions.¹² Magnon–phonon processes derive from spin orbit interactions which change as the direction of \mathbf{M} changes relative to the crystallographic axes. Magnon–magnon processes will also change with θ_M because of the shift in the spin wave band position.¹³ Any linewidth contribution associated with these processes would change as \mathbf{M} is pulled out of the easy crystallographic plane for the Zn–Y disk.

Specific connections are possible. Figure 5 of Ref. 13 shows a FMR linewidth ΔH_0 vs θ_M profile which has the same basic shape as the response in Fig. 7. Reference 13 set forth qualitative explanations for this response in terms of two magnon processes. There was, however, very limited quantitative agreement between the two magnon analysis and the data. The match-up in the ΔH_k vs θ_M profiles in Fig. 7 and the Fig. 5 data in Ref. 13 suggests an alternative explanation. Two magnon processes should *not* have a large effect on the spin wave linewidth,¹⁰ especially in single crystals.

If the ΔH_k vs θ_M profile in Fig. 7 and the ΔH_0 vs θ_M result from Ref. 13 do, in fact, have a common origin, one could argue that two magnon processes are not involved. Rather, the common mechanism should be related to the large magnetocrystalline anisotropy, spin orbit coupling, and magnon–phonon processes. A connection with spin orbit processes and magnon–phonon relaxation is certainly plausible here. The large anisotropy for the Zn–Y material originates from a very strong spin orbit interaction in the first place. Moreover, it is well known that a strong spin orbit interaction causes an increase in both the FMR linewidth and the spin wave linewidth. In order to understand the increase in ΔH_k one has to know the influence of the large anisotropy on spin wave and FMR damping. This influence has not been established yet quantitatively for easy plane and easy axis hexagonal ferrites. Even for well known uniaxial Ba–M hexagonal ferrite, the large values of the experimental FMR linewidth have not been quantitatively explained.¹⁴ Therefore, we can only speculate about the origin of the ΔH_k increase.

It is important to emphasize here that the results in Fig. 7 constitute the first observation of an angular dependence for the *spin wave linewidth* in any magnetic materials. There

have also been no previous theoretical predictions of such an effect and the exact mechanism has yet to be elucidated. The impact of this effect may be far reaching. One can expect, for example, a similar ΔH_k response in other high anisotropy materials such as uniaxial Ba–M hexagonal ferrite. In fact, the FMR linewidth in Ba–M disks shows an angular dependence which is similar to that found for Zn–Y.¹³ This discovery may also be relevant to large angle switching experiments in anisotropic materials. The data here suggest that the applicable damping will change as the magnetization vector changes its direction relative to the crystal axes during switching.

IV. SUMMARY AND CONCLUSION

The objective of this work was to examine the spin wave linewidth ΔH_k in thin disk samples of high anisotropy Zn–Y hexagonal ferrite and determine if ΔH_k is isotropic and wave vector \mathbf{k} independent, or if ΔH_k depends on the critical mode spin wave propagation direction or wave number k . Two classes of pumping configurations were used, one with the slab magnetized in plane (IPFOP case) and one with the magnetization pulled out of the disk plane (OPFOP case). Detailed measurements and analyses were made in the IPFOP case for a full range of angles between the in-plane magnetization and the microwave field, and in the OPFOP case for a full range of static field angles from in plane to perpendicular to plane.

For all of these geometries, experimental first order spin wave instability butterfly curves of the threshold microwave field amplitude h_{crit} versus the static field H were obtained for a pumping frequency of 16.7 GHz. Computed butterfly curves based on the formalism of Ref. 9 were then obtained for comparison with the data.

It was found that all of the IPFOP case data could be modeled in terms of a constant value of the spin wave linewidth $\Delta H_k = 12.8$ Oe. There was no systematic correlation between the h_{crit} data and the critical mode wave vector \mathbf{k} directions. It was found that the best fits to the data were always for $k \approx 0$. The OPFOP data showed a somewhat different result. In this case, the analysis gives good theoretical fits only if ΔH_k is increased as the magnetization \mathbf{M} is pulled out of plane. However, there was still no correlation between ΔH_k and the computed critical modes. The data suggest that the increase in ΔH_k as \mathbf{M} is pulled out of plane can be related to spin orbit coupling.

ACKNOWLEDGMENTS

This work was supported by the United States Office of Naval Research (ONR), Grant Nos. N00014-94-1-0096 and N00014-03-1-0070. The Zn–Y materials were grown by Dr. M. A. Wittenauer at Purdue University under ONR Grant No. N00014-91-J-1323. The authors are grateful to Dr. R. E. Eykholt for helpful discussions.

¹J. D. Adam, L. E. Davis, J. F. Dionne, E. F. Schloemann, and S. N. Stitzer, IEEE Trans. Microwave Theory Tech. **MTT-50**, 721 (2002); C. Vittoria, J. Magn. Magn. Mater. **21**, 109 (1980).

²J. J. Green and B. J. Healy, J. Appl. Phys. **34**, 1285 (1963).

³E. Schlömann, R. I. Joseph, and I. Bady, J. Appl. Phys. **34**, 672 (1963).

- ⁴R. G. Cox, C. E. Patton, M. A. Wittenauer, P. Kabos, and L. Chen, *J. Appl. Phys.* **89**, 4454 (2001).
- ⁵A. V. Nazarov, R. G. Cox, and C. E. Patton, *J. Appl. Phys.* **92**, 3890 (2002).
- ⁶J. J. Green, C. E. Patton, and E. Stern, *J. Appl. Phys.* **40**, 172 (1969).
- ⁷M. P. Dorsey, K. Sun, C. Vittoria, M. A. Wittenauer, F. J. Friedlander, and A. Schindler, *J. Appl. Phys.* **67**, 5524 (1990).
- ⁸A. V. Nazarov, Ph.D. thesis, Department of Physics, Colorado State University, 2002.
- ⁹A. V. Nazarov, C. E. Patton, R. G. Cox, L. Chen, and P. Kabos, *J. Magn. Mater.* **248**, 164 (2002).
- ¹⁰M. Sparks, *Ferromagnetic Relaxation Theory* (McGraw-Hill, New York, 1964).
- ¹¹A. G. Gurevich, A. V. Nazarov, O. A. Chivileva, and V. V. Petrov, *Phys. Solid State* **41**, 1513 (1999).
- ¹²A. G. Gurevich and G. A. Melkov, *Magnetization Oscillations and Waves* (CRC Press, Boca Raton, FL, 1996).
- ¹³M. J. Hurben, D. R. Franklin, and C. E. Patton, *J. Appl. Phys.* **81**, 7458 (1997).
- ¹⁴S. V. Lebedev, C. E. Patton, M. A. Wittenauer, L. V. Saraf, and R. Ramesh, *J. Appl. Phys.* **91**, 4426 (2002).